Terminal Mo Carbide and Carbyne Reactivity: H_2 Cleavage, B–C Bond Activation, and C–C Coupling

Gwendolyn A. Bailey and Theodor Agapie*

Division of Chemistry and Chemical Engineering, California Institute of Technology, 1200 E. California Blvd. MC 127-72, Pasadena, CA, USA

Supporting Information

Contents

I. EXPERIMENTAL DETAILS

General Considerations

All operations were carried out under a nitrogen atmosphere in an MBraun drybox or using standard Schlenk techniques. Solvents were dried over sodium benzophenone ketyl, or by the method of Grubbs.[1] Solvents, once dried and degassed, were stored under inert atmosphere over 4 Å molecular sieves. Methylidyne **2** and carbide **1** were prepared according to literature procedures.[2] CO (gas, ≥99%; Sigma-Aldrich), BPh_3 (Sigma Aldrich), and $BMes_3$ (Sigma Aldrich) were used as received. $NaBPh_4$ (Oakwood Chemicals) was dried at 60 °C in vacuo for 16 h. NMR spectra were recorded on a Bruker 400 MHz spectrometer (Prodigy broadband cryoprobe or broadband iProbe) or Varian 400 MHz spectrometer (broadband auto-tune OneProbe). Chemical shifts are reported in parts per million (ppm). ^{1}H and $^{13}C\{^{1}H\}$ chemical shifts are referenced to residual solvent peaks,[3] $^{31}P\{^{1}H\}$ chemical shifts are referenced to an external sample of 85% H_3PO_4 (0 ppm), and ^{2}H chemical shifts are referenced internally to C_6D_6 (spiked into the reaction mixture; 7.16 ppm). Multiplicities are abbreviated as follows: s = singlet, d = doublet, t = triplet, dd = doublet of doublets, dt = doublet of triplets, td = triplet of doublets, m = multiplet, br = broad. Infrared (IR) spectra were collected on a Thermo Fischer Nicolet 6700 FTIR spectrometer. Elemental analysis was performed using a PerkinElmer 2400 Series II CHN Elemental Analyzer.

H_2 gas (Airgas; 99.9%) and D_2 gas (Cambridge Isotopes; 99.8%) were rigorously dried by immersion (3/4 height) of a sealed 1 L round bottom flask at 1 atm in liquid N_2 for 3 min. The gas was then transferred to the reaction flask via an oven-dried transfer bridge. > ***Safety hazard***: Condensation of water in a sealed flask at cryogenic temperatures poses a significant safety hazard in case there is a leak in the setup, since O_2 from the atmosphere may condense in the trap and subsequently explode. To minimize the explosion hazard, the trap setup should be rigorously leak-checked and the drying time should be minimized (3-5 min is sufficient to ensure drying, while minimizing potential O_2 condensation hazard). Additionally, the setup should be contained behind a blast shield at all times.

H_2 splitting with carbide 1

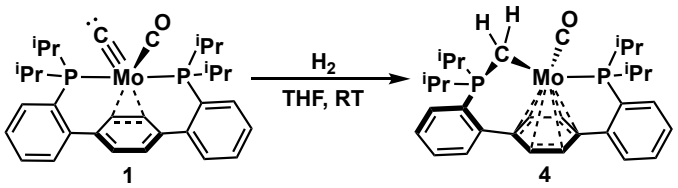

After degassing via three consecutive freeze/pump/thaw cycles, a cold in situ-generated solution of **1** (0.047 mmol in 1.5 mL THF) in a 10 mL reaction vessel was subjected to pre-dried H_2 (1 atm) and then warmed to RT. After temperature equilibration, the vessel was sealed shut using a Kontes valve and the solution was stirred at RT for 20 h. $^{31}P\{^{1}H\}$ NMR (202 MHz, THF, 23 °C; Figure S1): 89.0 (br s; ca. 10%), 88.1 (s; minor) 85.3 (d, $^{4}J_{PP}$ = 17.4 Hz,

Mo–*P* of **4**; 9%), 82.4 (s; 10%), 77.4 (d, J = 21.8 MHz; 4%), 77.1 (d, J = 21. 8 MHz; 4%), 48.9 (d, $^4J_{PP}$ = 17.5 Hz, Mo–CH_2*P* of **4**; 11%), -3.5 (free P2; 34%), -4.3 (s; 19%). $^{31}P\{^1H\}$ NMR chemical shifts and J-couplings for **4** matched those of an independently prepared sample in THF (Figure S1d).[2]

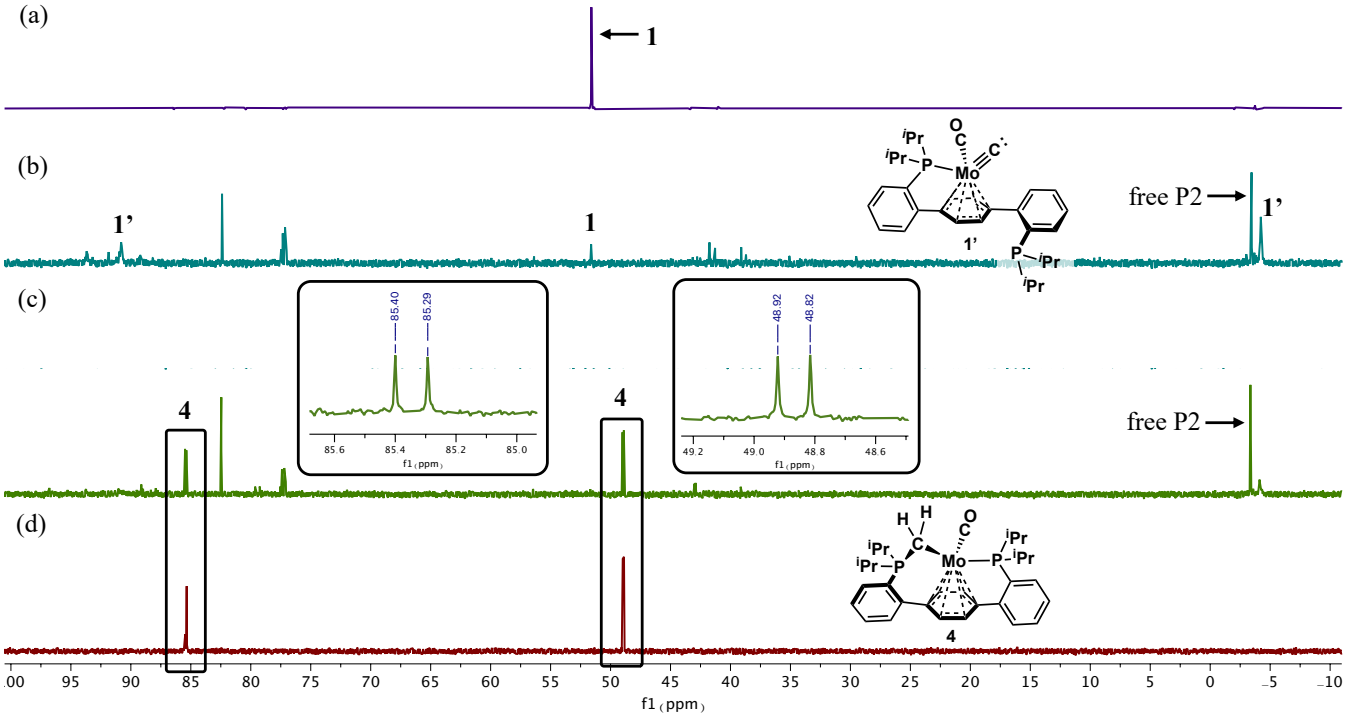

Figure S1—$^{31}P\{^1H\}$ NMR spectra (202 MHz, THF, 23 °C) showing (a) clean carbide **1**, prior to addition of H_2; (b) carbide **1** in the absence of H_2 (t = 18 h); (c) the reaction of carbide **1** + H_2 (t = 18 h); (d) clean **4** (independently prepared[2]).

Similar results were obtained on reaction of **1** with D_2 under identical conditions, only the proportion of the impurity signal at δ_P 82.38 was increased (Figure S2). ^2H NMR (61 MHz, THF, 23 °C; Figure S3): 3.44 (s, THF), 1.59 (s, THF + unidentified), 1.07 (s, P–CD_2 of **4**), 0.55 (s, P–CD_2 of **4**). The solvent peaks (THF-H_8) complicate analysis of the ^1H NMR spectrum, so that absence of the P–CH_2 peaks could not be discerned. Repeating the same reaction in the absence of H_2/D_2, **4** was not observed, though several of the products formed were the same. Consistent with previous results,[2] the primary species identified was carbide **1'**, PMo(C:)(CO)P, an isomer of **1** in which one phosphine arm has become unbound and the central arene moiety is bound in an η_6 fashion. $^{31}P\{^1H\}$ NMR (202 MHz, THF, 23 °C; Figure S1c): 90.8 (br s, Mo–P of **1'**), 82.4 (s), 77.4 (d, J = 21.8 MHz), 77.1 (d, J = 21. 8 MHz), 48.9 (d, $^4J_{PP}$ = 17.5 Hz, Mo–CH_2*P* of **4**), -3.5 (free P2), -4.2 (br s, free phosphine arm of **1'**).

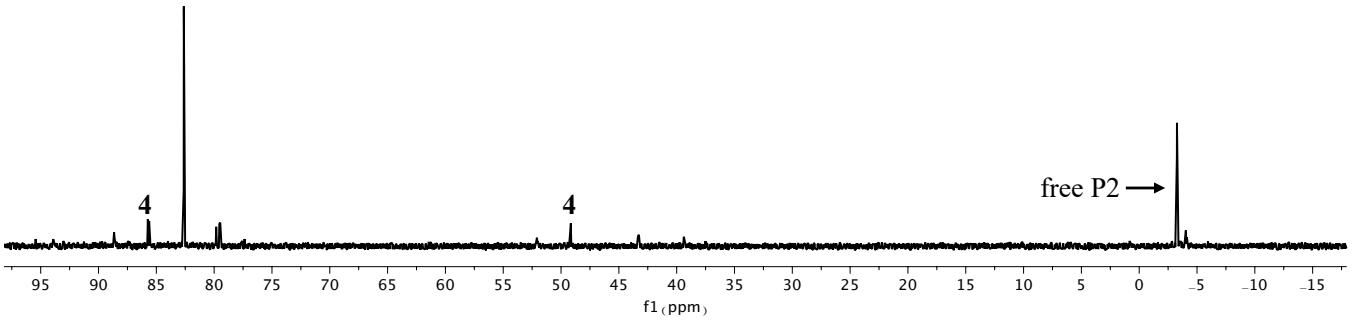

Figure S2—$^{31}P\{^1H\}$ NMR spectrum (202 MHz, THF, 23 °C) showing products formed on reaction of carbide **1** with D_2.

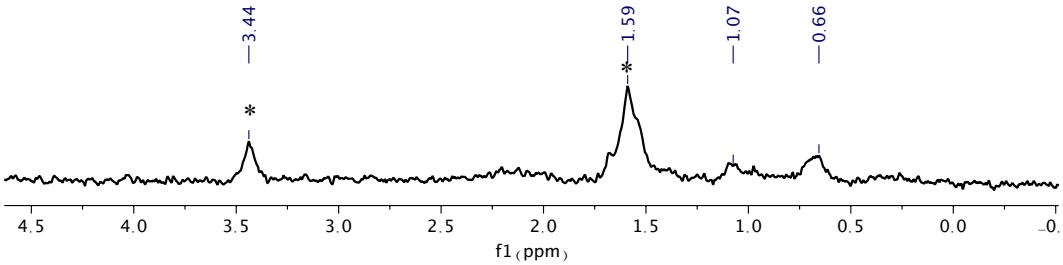

Figure S3—^{2}H NMR spectrum (61 MHz, THF, 23 °C) showing appearance of key methylene-d_2 signals (δ 1.07, 0.66) for **4** on treatment of carbide **1** with D_2. Asterisks (*) indicate the THF solvent (natural abundance ^{2}H); the signal at 1.59 is likely overlapping with an unidentified impurity.

KCl-free control experiments. KCl-free carbide **1** was generated by pumping down cold solutions of **1** (kept <0 °C in a liquid N_2-chilled cold well), extracting into thawing C_6H_6, and lyophilizing. Subjecting to 1 atm H_2 as above yielded clear orange solutions and an insoluble pink precipitate. $^{31}P\{^{1}H\}$ NMR (orange solution, 202 MHz, THF, 23 °C): silent.

Borylcarbene 6 and intermediate borane adduct 5

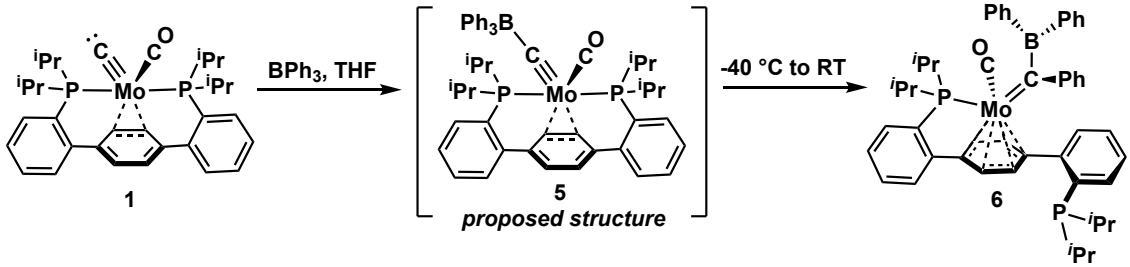

*In situ observation of intermediate **5**:* To a freshly prepared thawing solution of carbide **1** (0.062 mmol) in THF (1.5 mL) was added BPh_3 (15.3 mg, 0.062 mmol, 1 equiv) in THF (0.5 mL). A slight lightening of the deep red color was observed during the addition. An aliquot was taken for NMR analysis and warmed to -20 °C inside the probe. $^{31}P\{^{1}H\}$ NMR (202 MHz, THF, –20 °C; Figure S4): 43.2 (s), -6.29 (s; minor impurity). ^{11}B NMR (C_6D_6, 128 MHz, 23 °C): no signals. $^{13}C\{^{1}H\}$ NMR (C_6D_6, 101 MHz, 23 °C; Figure S5): 157.21 (br s, Mo–*C*O), 147.85 (t, J_{PC} = 6.2 Hz, aryl-*C*), 138.01 (t, J_{PC} = 3.2 Hz, aryl-*C*), 137.39 (s, aryl-*C*), 135.14 (s, aryl-*C*), 132.20 (s, aryl-*C*), 130.37 (s, aryl-*C*), 128.70 (s, aryl--*C*), 128.67 (s, aryl-*C*), 128.28 (s, aryl-*C*), 128.05 (s, aryl-*C*), 127.92 (s, aryl-*C*). 125.48 (s, aryl-*C*), 125.05 (s, aryl-*C*), 122.57 (s, aryl-*C*), 29.63 (s, –*C*H(CH$_3$)$_2$), 27.73 (d, J_{PC} = 7.4 Hz, –*C*H(CH$_3$)$_2$), 27.64 (d, J_{PC} = 8.6 Hz, –*C*H(CH$_3$)$_2$), 20.51 (d, J_{PC} = 8.7 Hz, –*C*H(CH$_3$)$_2$), 19.29 (s, –CH(*C*H$_3$)$_2$), 18.67 (s, –CH(*C*H$_3$)$_2$), 18.24 (s, –CH(*C*H$_3$)$_2$), 17.54 (s, –CH(*C*H$_3$)$_2$), 13.59 (s, –CH(*C*H$_3$)$_2$). No signals were detected in the $^{13}C\{^{1}H\}$ NMR spectrum in the region from 592-162 ppm, nor in the ^{11}B NMR spectrum from 100 ≥ δ ≥ -100 ppm. Likewise, in a ^{1}H – ^{13}C HMQC experiment, the carbide ^{13}C signal was not detected in the region from 570-162 ppm. The carbide ^{13}C signals and the ^{11}*B*Ph$_3$ signals may be masked at this temperature due to broadness.

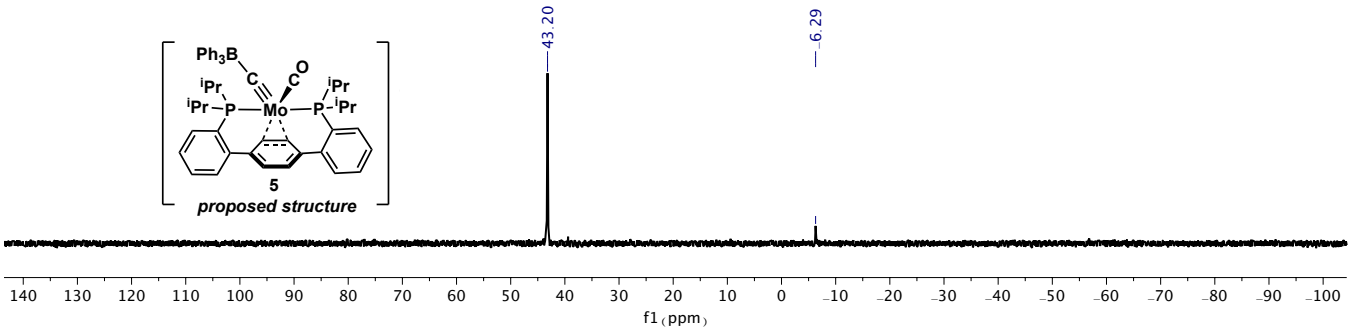

Figure S4—$^{31}P\{^{1}H\}$ NMR spectrum (202 MHz, THF, –20 °C) of intermediate **5**.

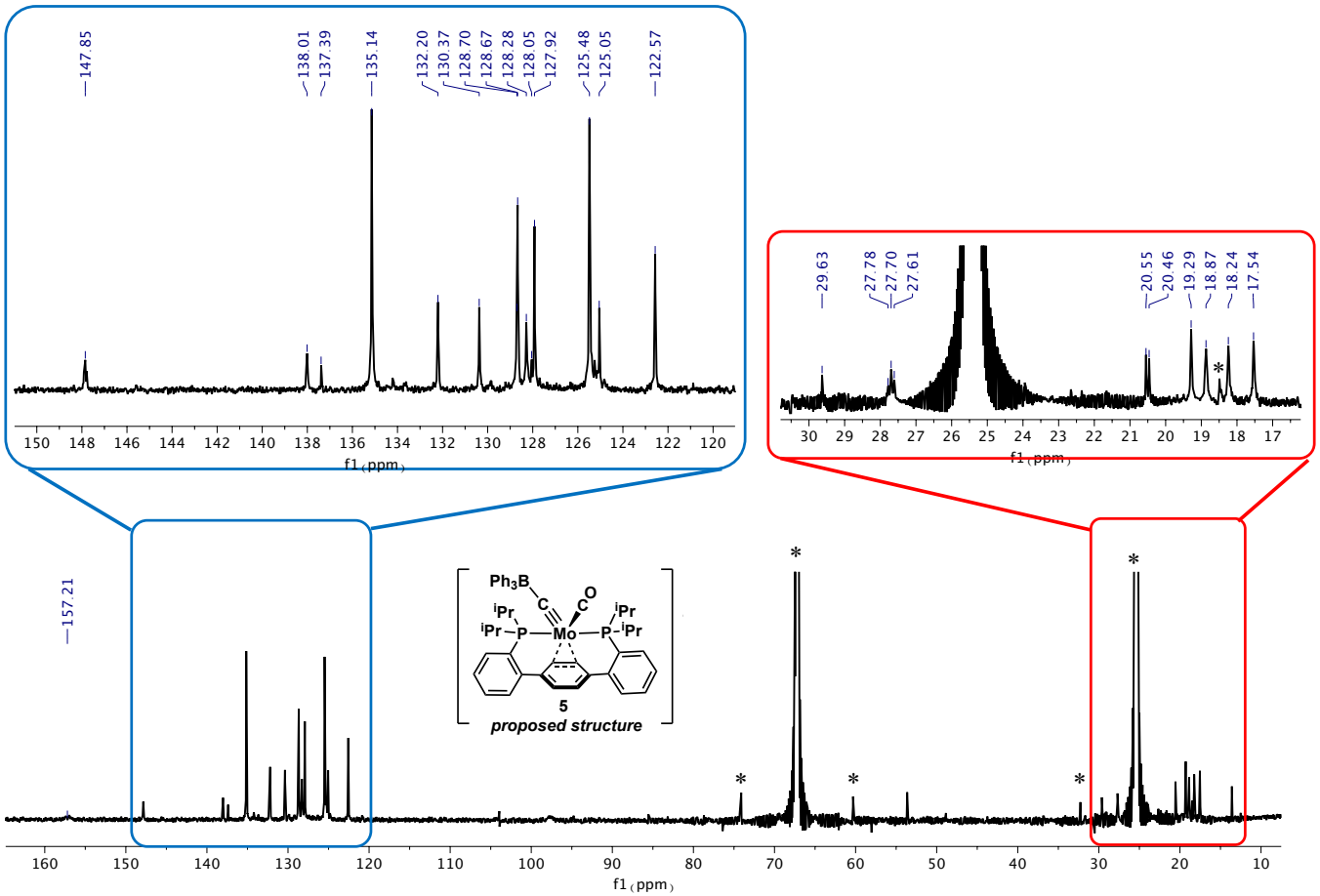

Figure S5—$^{13}C\{^{1}H\}$ NMR spectrum (126 MHz, C_6D_6, 23 °C) of intermediate **5**. (*) indicates solvent peaks (THF).

Conversion to borylcarbene ***6***. The solution from above was allowed to warm to RT, over which time a color change from deep red to brown occurred. $^{31}P\{^{1}H\}$ NMR spectra taken at RT over 4 h revealed consumption of this intermediate species, and gradual conversion to **6**. $^{31}P\{^{1}H\}$ NMR (THF, 202 MHz, 23 °C, t = 2 h; Figure S6): 76.2 (s, Mo–*P* of **6**, major), 43.2 (s, **5**, minor), -5.0 (s, free *P*^{i}Pr$_2$ of **6**, major), -5.4 (s, free P2, minor).

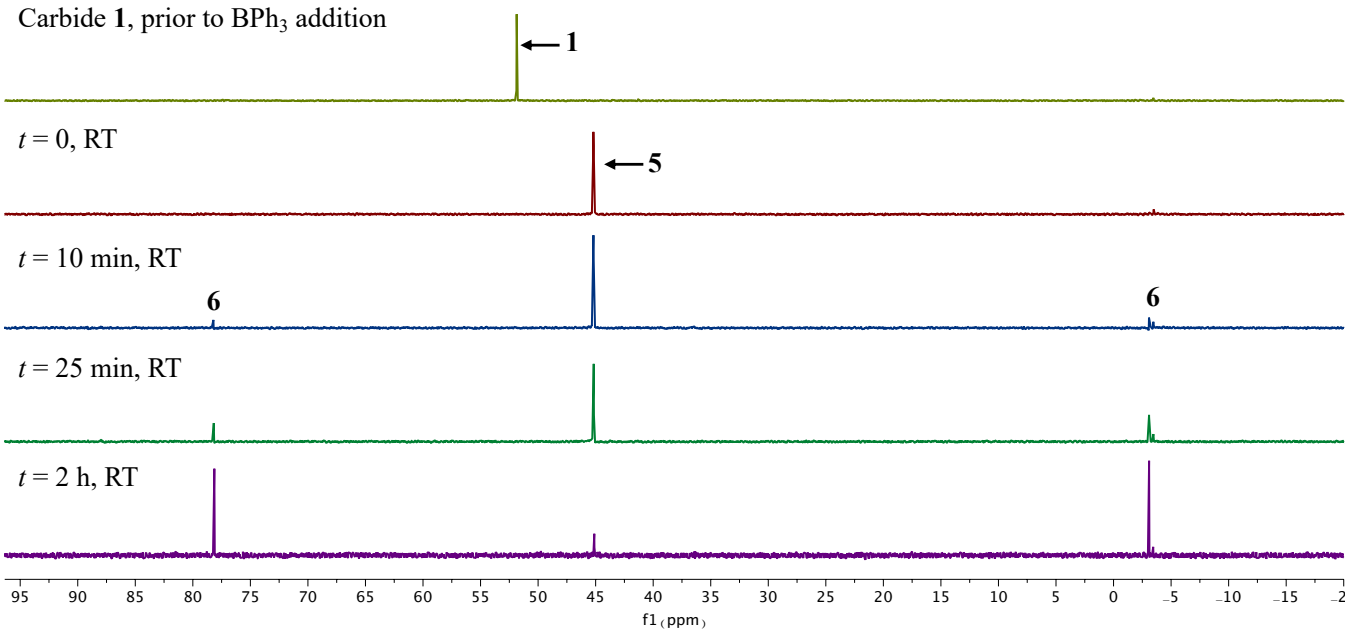

Figure S6—$^{31}P\{^{1}H\}$ (202 MHz, THF, 23 °C) NMR spectra showing the conversion of carbide **1** to borylcarbene **6** via intermediate **5**.

Preparation of borylcarbene **6**. This reaction was conducted as above, but with 0.125 mmol carbide **1**, BPh_3 (30.5 mg, 0.125 mol), and THF (4 mL). After addition of the BPh_3, the solution was allowed to warm to RT, prompting a color change from deep red to brown. After 4 h, the reaction was concentrated in vacuo and the resulting oily solid was suspended three times with vigorous stirring in hexanes (2 mL), concentrating each time to remove residual THF. After extracting into benzene (6 mL) and lyophilizing, the product was crystallized by vapor diffusion of pentane into THF solutions. Filtration and drying in vacuo afforded 6 as a dark brown crystalline solid (61 mg, 58%). ^{1}H NMR (C_6D_6, 400 MHz, 23 °C; Figure S7): 8.04 (dd, J = 23.6 Hz, J = 7.6 Hz, 4H, BPh_2 *o*-C*H*), 7.59–7.09 (overlapping m, 8H, aryl *H*), 7.00–6.69 (overlapping m, 9H, aryl *H*), 5.66 (d, J = 5.6 Hz, 1H, central arene–*H*), 5.24 (d, J = 6.0 Hz, 1H, central arene–*H*), 2.00–1.83 (m, 1H, C*H*$(CH_3)_2$) 1.79–1.61 (m, 3H, C*H*$(CH_3)_2$). 1.32–1.17 (m, 1H, C*H*$(CH_3)_2$), 1.17–1.06 (m, 3H, CH(C*H*$_3)_2$), 1.04–0.82 (m, 9H, CH(C*H*$_3)_2$), 0.81–0.52 (m, 12H, CH(C*H*$_3)_2$). $^{31}P\{^{1}H\}$ NMR (C_6D_6, 202 MHz, 23 °C; Figure S8): 77.4 (s), -4.2 (s). ^{11}B NMR (C_6D_6, 128 MHz, 23 °C): no signals. $^{13}C\{^{1}H\}$ NMR (C_6D_6, 101 MHz, 23 °C; Figure S9): 242.13 (s, Mo–*C*O), 151.08 (s, aryl-*C*), 144.60 (d, J = 19.9 Hz, aryl-*C*), 143.87 (d, J = 10.6 Hz, aryl-*C*), 143.61 (d, J = 5.6 Hz, aryl-*C*), 136.24 (d, J = 33.1 Hz, aryl-*C*), 134.35 (d, J = 23.4 Hz, aryl-*C*), 133.09 (d, J = 4.8 Hz, aryl-*C*), 131.87 (d, J = 2.7 Hz, aryl-*C*), 129.84 (s, aryl-*C*), 129.37 (d, J = 1.3 Hz, aryl-*C*) 128.92 (s, aryl-*C*). 128.78 (d, J = 37.6 Hz, aryl-*C*), 127.07 (s, aryl-*C*), 126.75 (d, J = 9.4 Hz, aryl-*C*), 126.52 (s, aryl-*C*), 126.09 (s, aryl-*C*), 125.79 (s, aryl-*C*), 124.05 (s, aryl-*C*), 123.37 (d, J = 4.3 Hz, aryl-*C*), 110.32 (2 d, J = 4.5 Hz, central arene-*C*), 106.60 (d, J = 6.8 Hz, central arene-*C*), 100.96 (d, J = 14.9 Hz, central arene-*C*), 94.20 (d, J = 38.0 Hz, central arene-*C*), 29.22 (d, J = 18.5 Hz, –*C*H$(CH_3)_2$), 27.54 (d, J = 22.1 Hz, –*C*H$(CH_3)_2$), 26.34 (d, J = 15.6 Hz, –*C*H$(CH_3)_2$), 25.00 (d, J = 13.5 Hz, –*C*H$(CH_3)_2$), 20.45 (d, J = 29.9 Hz, –CH(*C*H$_3)_2$), 20.28 (d, J = 22.4 Hz, –CH(*C*H$_3)_2$), 19.61 (d, J = 4.4 Hz, –CH(*C*H$_3)_2$), 18.92 (d, J = 7.7 Hz, –CH(*C*H$_3)_2$), 18.53 (d, J = 3.0 Hz, –CH(*C*H$_3)_2$), 18.15 (s, –CH(*C*H$_3)_2$), 16.89 (d, J = 3.5 Hz, –CH(*C*H$_3)_2$), 13.92 (s, –CH(*C*H$_3)_2$). The carbene ^{13}C resonance was detected via ^{1}H – ^{13}C HMQC (C_6D_6, 23 °C): 346.15 (s, Mo=*C*). IR (solution in THF, cm^{-1}): 1802. Anal. calcd (%) for $C_{50}H_{55}BMoOP_2$ (M_w = 840.70): C, 71.43; H, 6.59. Found: C, 71.73; H, 6.47. Crystals for single crystal X-ray diffraction studies were grown by vapor diffusion of pentane into THF solutions.

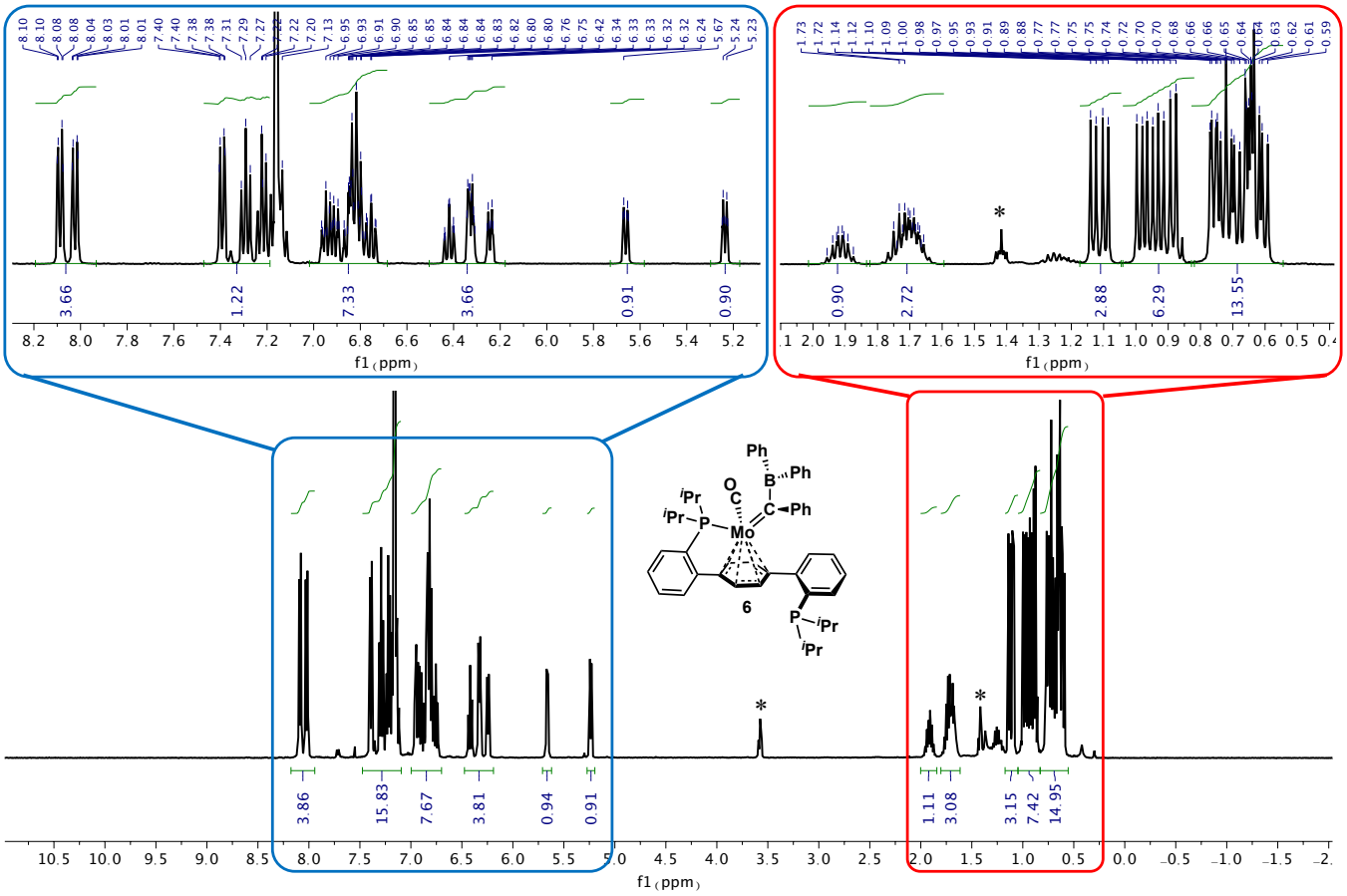

Figure S7—^{1}H NMR spectrum (400 MHz, C_6D_6, 23 °C) of **6** (* denotes residual THF).

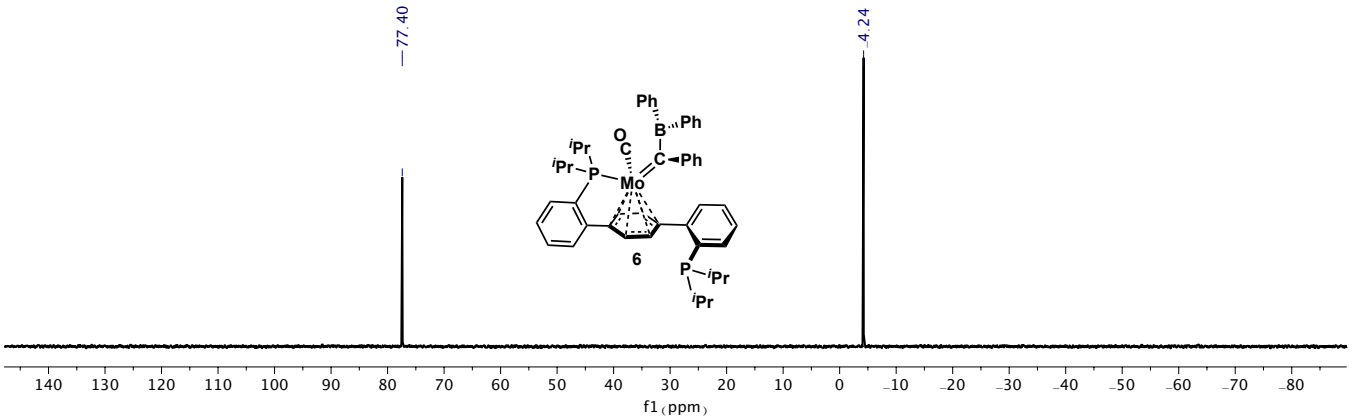

Figure S8—^{31}P{^{1}H} NMR spectrum (202 MHz, C_6D_6, 23 °C) of **6**.

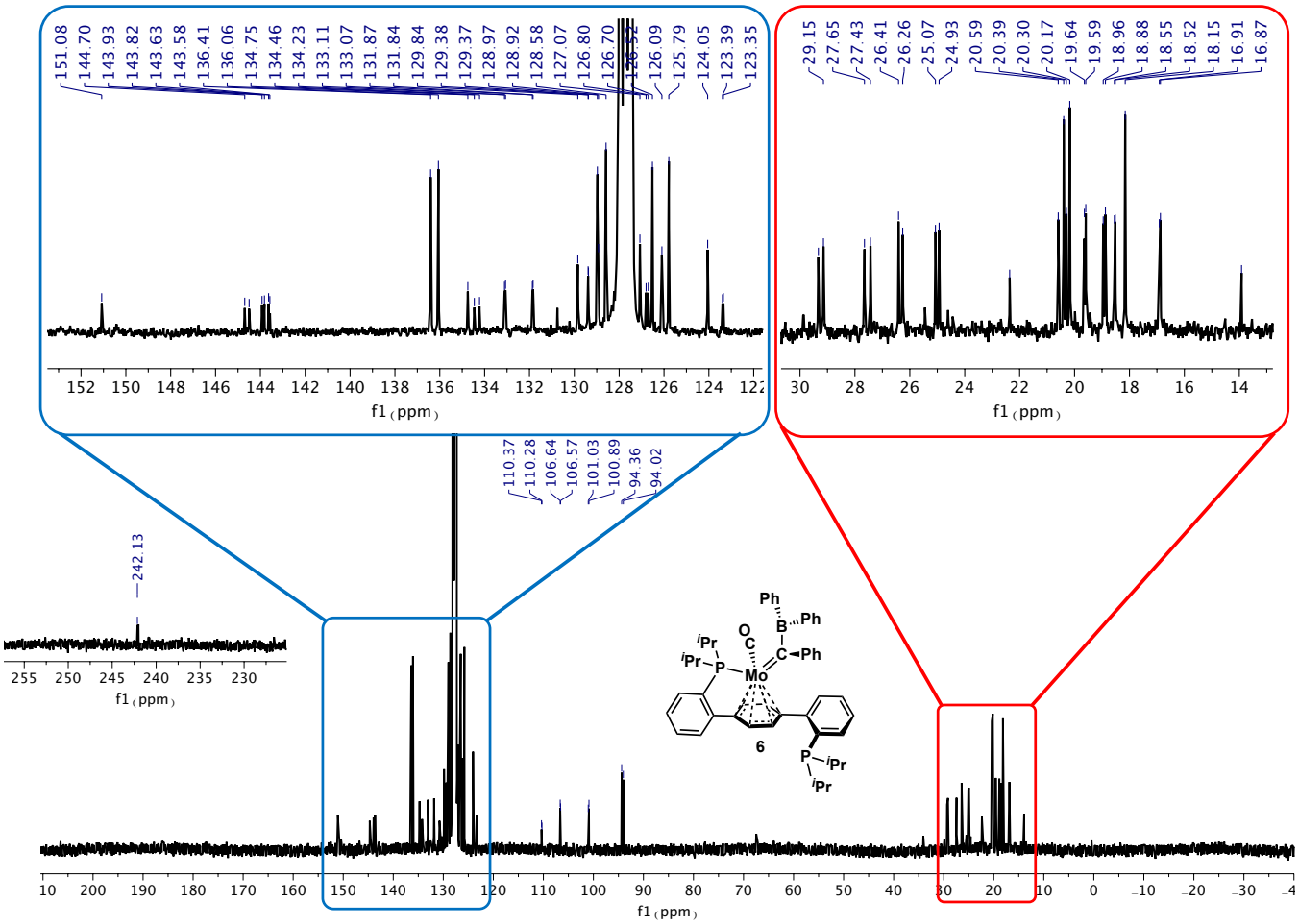

Figure S9—$^{13}C\{^{1}H\}$ NMR spectrum (126 MHz, C_6D_6, 23 °C) of **6**.

C–C coupling of methylidyne 2'

Observation of ketenyl complex 7

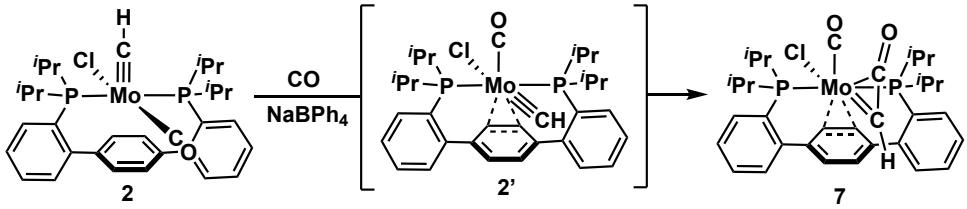

A solution of **2** (12.2 mg, 0.018 mmol) and $NaBPh_4$ (6.2 mg, 0.018 mmol, 1 equiv) in 600 µL THF in a J. Young tube was degassed (three consecutive freeze/pump/thaw cycles), and then the headspace was refilled with CO (1 atm).

Safety hazard: Handling of CO poses a significant safety threat to humans, owing to its toxicity and physical properties as a colorless, odorless, and tasteless gas. Victims may be rendered unconscious before realizing they have been poisoned. Besides unconsciousness, CO poisoning can cause weakness, dizziness, and nausea along with tachycarida and tachypnea (rapid heartbeat and breathing), and ultimately death. CO should be handled in a fumehood at all times with appropriate CO sensors in operation.

$^{31}P\{^{1}H\}$ NMR spectroscopy of the orange solution after 8 days revealed complete consumption of **2**, and formation of **2'**,[2] along with minor amounts of an unidentified species and trace free P2. $^{31}P\{^{1}H\}$ NMR (202 MHz, THF, 23 °C): 41.79 (s, **2'**, major), 34.68 (s, unidentified, minor), -3.34 (s, free P2, trace). The reaction was left at RT for 6 weeks, during which time brown, rod-like single crystals grew out of the orange solution. The insolubility of these crystals in common solvents (toluene, benzene, diethyl ether, THF) precluded analysis by NMR spectroscopy or other solution methods. Nonetheless, a single crystal X-ray diffraction study confirmed the identity of these crystals as ketenyl complex **7** (for details, see section III).

Subsequent attempts to prepare 7 on more reasonable time and material scales proved unsuccessful. Thus, a solution of **2** (30 mg, 0.045 mmol) and $NaBPh_4$ (15.5 mg, 0.045 mmol, 1 equiv) in THF (0.7 mL) under a headspace of CO (1 atm) in a J. Young tube was heated to 60 °C. A color change from orange to brown was observed over a period of days, but no insoluble species crystallized on cooling to RT. $^{31}P\{^{1}H\}$ NMR analysis indicated conversion of **2** to **2'**, followed by decomposition to an intractable mixture of unidentified species. $^{31}P\{^{1}H\}$ NMR (202 MHz, THF, 23 °C, t = 7 days; major species only; Figure S10a): 85.14 (s, unidentified), 47.82 (s, unidentified), 41.76 (s, **2'**); numerous other unidentified minor species were also observed, but not listed here. In another experiment, a solution of **2'** (ca. 28 mg) in toluene (0.7 mL) was heated to 80 °C under 1 atm CO in a J. Young tube. In this experiment, the poor solubility of $NaBPh_4$ in toluene precluded its inclusion in the reaction mixture. $^{31}P\{^{1}H\}$ NMR analysis at 12 h revealed that **2'** was the major product of the reaction, though some unidentified species were also formed. A THF-insoluble brown film was observed around the surface of the tube. $^{31}P\{^{1}H\}$ NMR (202 MHz, THF, 23 °C, t = 12 h; major species only; Figure S10b): 41.76 (s, major, **2'**), 41.26 (s, minor remaining **2**), 34.98 (s, minor, unidentified), 26.10 (s, minor, unidentified), -4.10 (s, minor, unidentified), -4.29 (s, minor, unidentified).

In a final experiment, **2** (50 mg, 0.079 mmol) and $NaBPh_4$ (25.8 mg, 0.079 mmol, 1 equiv) in THF (1.2 mL) were reacted under CO in a 10 mL reaction tube sealed with a teflon (Kontes) valve. After 2 months, the filtered yield of brown crystals was ca. 1 mg, precluding characterization by combustion analysis or other methods.

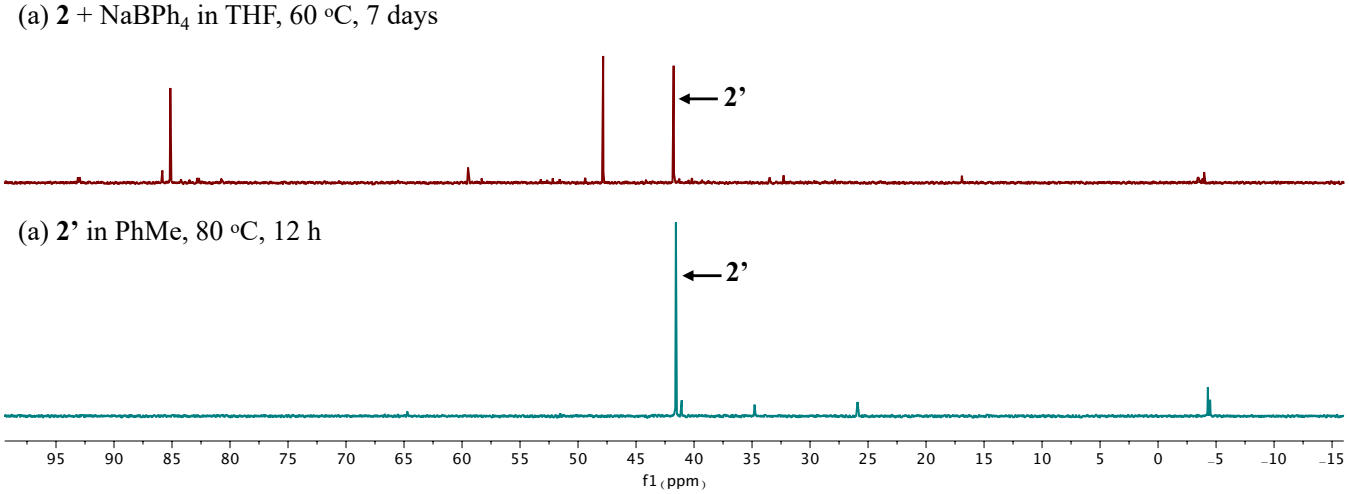

Figure S10—$^{31}P\{^{1}H\}$ NMR spectra (202 MHz, THF, 23 °C) showing attempted syntheses of ketenyl complex **7** on a reasonable time scale. (a) **2** and $NaBPh_4$ under CO in THF, 60 °C. (b) **2'** under CO in toluene, 80 °C.

Table S1—Comparison of key bond lengths (Å) and angles (°) for η^2-C,C-ketenyl complex 7, η^1-ketenyl complex 8, free ketene, and previously reported non-terminal η^2-C,C-ketenyl complexes. [a,b]

	7	8	ketene[4]	9[5]	lit. range [a]
Mo1–C32	1.958(5)	2.290(2)	-	2.009(5)	2.002(4)[c]
Mo1–C33	2.180(5)	2.840(7)	-	2.034(4)	2.210(4)[c]
C32–C33	**1.302(7)**	1.289(1)	1.314	1.316(6)	1.32–1.41
C33–O2	1.221(6)	1.186(1)	1.161	-	1.20–1.32
Mo1–C31	1.925(4)	1.956(1)	-	-	-
C31–O1	1.159(5)	1.169(1)	-	-	-
C32–C33–O2	152.3(5)	179.02(7)	-	-	139–153
Mo1–C32–C33	**81.3(3)**	101.34(4)	-	-	65–77

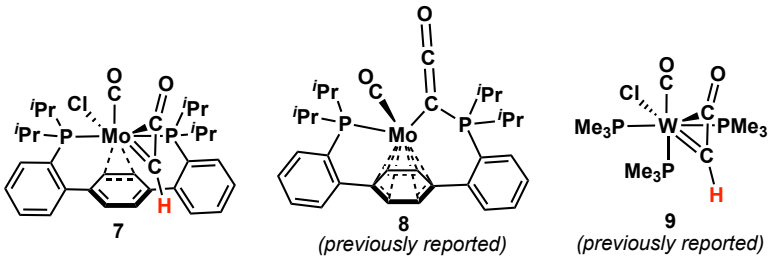

[a] Range of equivalent bond lengths and angles reported for crystallographically characterized η^2-C,C-ketenyl complexes of Mo or W.[6] The structure of complex η^1-ketenyl complex **8** is drawn in Chart S1. For atom numbering scheme, see Figure S16.
[b] Bond lengths and angles that deviate most significantly from non-terminal literature examples are emphasized in bold.
[c] Only one previously reported example exists for Mo;[6f] all other examples are with W. The W–C(ketenyl) distances range from 1.97–2.03 Å and 2.02–2.21 Å for C_α and C_β, respectively.

Chart S1—Proposed resonance forms for ketenyl complex 7.

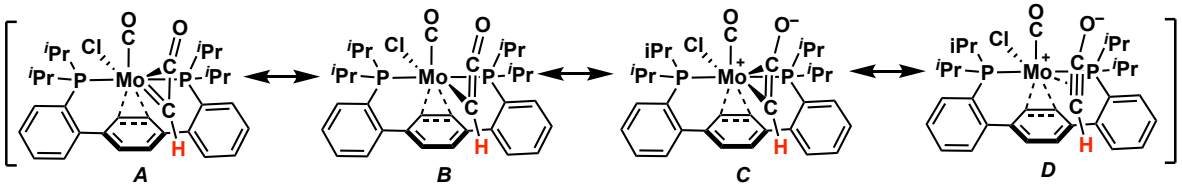

Calculation of hydricity requirement for H_2 cleavage by 1 + borane FLP

The hydricity requirement for thermoneutral H_2 cleavage by carbide **1** and a borane BR_3 as a Frustrated Lewis Pair was calculated using the previously estimated values for the effective pK_a of proton and chloride transfer to **1** (pK_a(Cl) ≥ 33 in THF)[2] and Gibbs free energy for heterolytic H_2 cleavage (Figure S11).[7] Solving for hydricity, we find that ΔG_{H^-} ($[HBR_3]^-$) = 76 – 45 = 31 kcal / mol. Thus, by these estimates, ΔG_{H^-} ($[HBR_3]^-$) must be greater than 31 kcal/mol for H_2 cleavage to be thermodynamically favored, at least at the lower limit of carbide basicity.

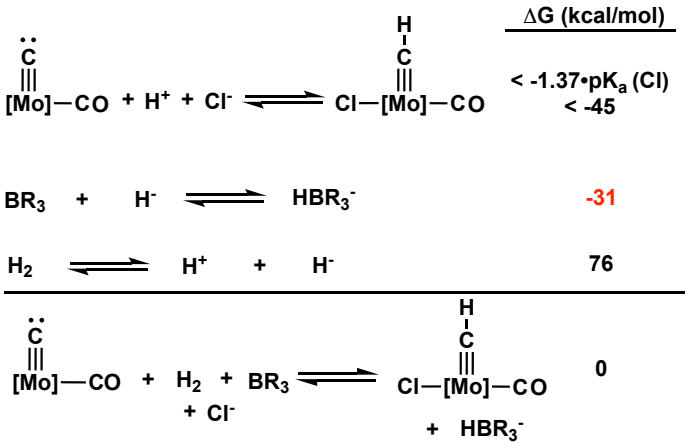

Figure S11. Thermodynamic scheme for thermoneutral H_2 cleavage by carbide **1** and borane.

COMPUTATIONAL DETAILS

General Considerations

Calculations were performed using density functional theory (DFT) as implemented in Gaussian 09, Revision C.01.[8] Geometry optimizations and electronic structure calculations were performed in Gusing the revised TPSS or BP86 exchange and correlation functionals,[9] using the LANL2DZ[10] or def2-TZVP[9] basis set for all atoms. Solvent corrections were applied in Gaussian using the Polarizable Continuum Model for benzene.[11-13] Optimizations were performed ignoring molecular symmetry, starting from crystallographic coordinates. To increase computational efficiency for the larger complex **6**, truncated ligand model with $-PMe_2$ substituents used in place of $-P^iPr_2$. Frequency calculations were performed on all optimized geometries to ensure true minima with real vibrational modes. Structures optimized in this fashion showed good agreement with bond lengths and angles determined via single crystal X-ray diffraction (Table S2, S3). Molecular orbitals were visualized using GaussView, the GUI component of the Gaussian software package, or UCSF Chimera.[14]

Borylcarbene 6

Table S2—Comparison of experimental and calculated bond lengths (Å) and angles (°) for 6.

	Exp.	Calc.		Exp.	Calc.
Mo1–C31	1.948(5)	1.9403	**B1–C35**	1.614(8)	1.5996
C31–O1	1.174(6)	1.2274	**C32–C33**	1.459(7)	1.4658
Mo1–C32	2.012(5)	2.0096	**Mo1–P1**	2.502(1)	2.5135
C32–B1	1.534(7)	1.5508	**Mo1–C_{arene} (avg)**	2.398(5)	2.4268
Mo1–B1	2.587(6)	2.6380	**C–C (arene, avg)**	1.412(7)	1.4397
Mo1–C33	3.273(5)	3.2008	**Mo1–C32–B1**	92.7(3)	94.74
B1–C34	1.599(8)	1.6143	**Mo1–C32–C35**	140.6(4)	133.54

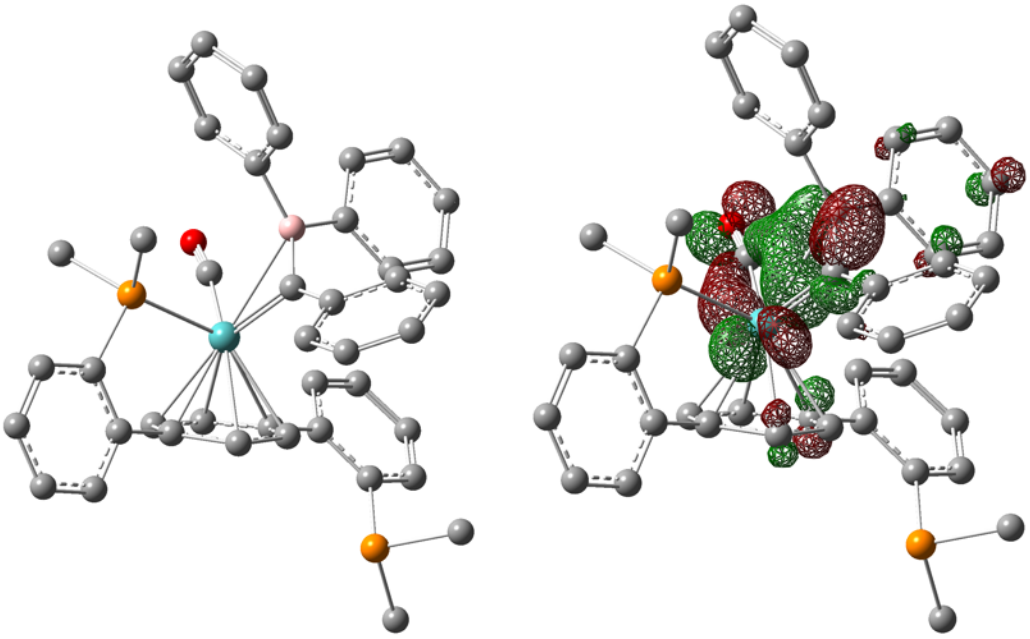

Figure S12—(a) DFT-optimized structure of borylcarbene **6** with radii scaled by 50%. (b) Calculated HOMO of borylcarbene **6** (isocontours 0.05 e^- $Å^{-4}$).

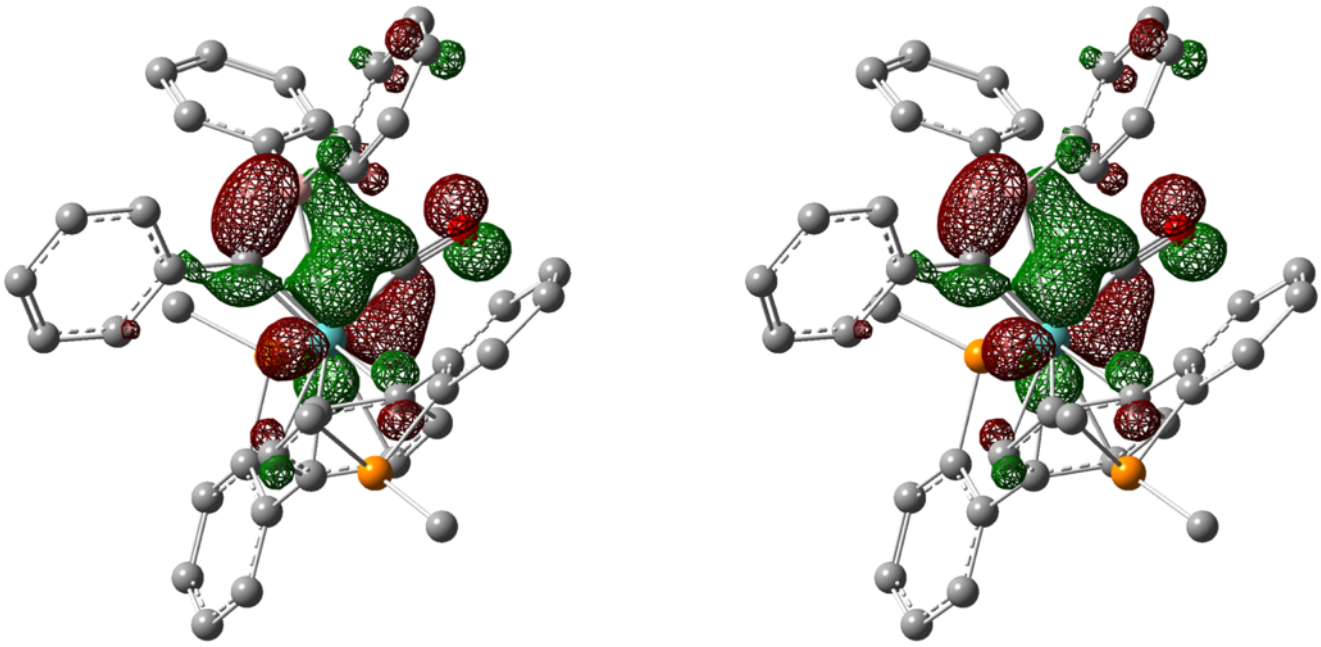

Figure S13—Stereographic pair for 3D viewing of HOMO of borylcarbene **6** (isocontours 0.05 e^{-} $Å^{-4}$).

Ketenyl complex 7

Table S3—Comparison of experimental and calculated bond lengths (Å) and angles (°) for 7.

	Exp.	Calc.		Exp.	Calc.
Mo1–C32	1.958(5)	1.9960	**Mo–P (avg.)**	2.592(1)	2.6283
Mo1–C33	2.180(5)	2.2708	**Mo1–C1**	2.596(4)	2.5964
C32–C33	1.302(7)	1.3460	**Mo1–C2**	2.596(4)	2.5970
C33–O2	1.221(6)	1.2119	**C1–C2**	1.388(6)	1.4031
Mo1–C31	1,925(4)	1.9222	**C4–C5**	1.390(6)	1.4089
C31–O1	1.159(5)	1.1711	**Mo1–C32–C33**	81.3(3)	83.17
Mo–Cl	2.504(1)	2.5055	**C32–C33–O2**	152.3(5)	155.26

[a] For atom numbering scheme, see Figure S16.

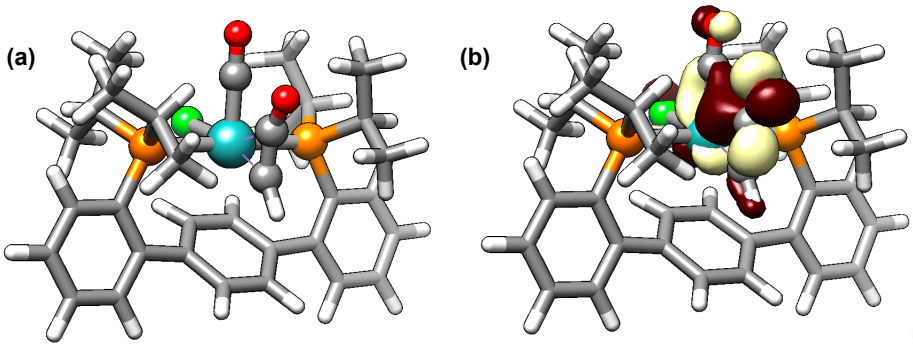

Figure S14—(a) DFT-optimized structure of ketenyl complex **7**. (b) Calculated HOMO for **5** showing Mo–C_{32} Z-interaction (isocontours 0.05 e^{-} $Å^{-4}$).

CRYSTALLOGRAPHIC INFORMATION

CCDC deposition numbers 2000078 and 2000079 contain the supplementary crystallographic data for this paper. These data can be obtained free of charge from the Cambridge Crystallographic Data Centre via www.ccdc.cam.ac.uk/data_request/cif.

Data Collection
Crystals were mounted on a MiTeGen loop using Paratone oil, and then placed on the diffractometer under a nitrogen stream. Low-temperature diffraction data (ϕ-and ω-scans) were obtained on a Bruker APEXII CCD-based diffractometer (Mo-K_α radiation or Cu-K_α radiation at λ = 0.71073 Å or λ = 1.54178 Å, respectively). All diffractometer manipulations, including data collection, integration, and scaling were carried out using the Bruker APEXIII software.[15] Absorption corrections were applied using SADABS,[16] unless otherwise noted. Space groups were determined on the basis of systematic absences and intensity statistics, and the structures were solved in the Olex^2 software interface[17] by intrinsic phasing using XT (incorporated into SHELXTL)[18] and refined to convergence by full-matrix least squares on F^2. All non-hydrogen atoms were refined using anisotropic displacement parameters. Hydrogen atoms were placed in the idealized positions and refined using a riding model, unless noted otherwise. Graphical representations of structures with 50% probability thermal ellipsoids were generated using the Diamond 3 visualization software.[19]

Special refinement details
The crystal used for **6** was twinned. The twin components were separated and assigned using the program CELL_NOW, and corrected for absorption using TWINABS.[20] The crystal structure was refined with racemic twinning as applied using a TWIN law with a batch scale factor (BASF) of 0.2.

Table S4—Crystal and refinement data for complexes **6** and **7**.

	6	**7**
CCDC Number	2000078	2000079
Empirical formula	$C_{50}H_{55}BMoOP_2$	$C_{37}H_{49}MoO_3P_2$
Formula weight	840.70	701.22
T (K)	100	100
***a*, Å**	9.4239(17)	12.8746(13)
***b*, Å**	12.722(2)	14.3843(18)
***c*, Å**	35.056(4)	18.874(2)
α, °	90	90
β, °	90	100.405(5)
γ, °	90	90
Volume, Å^3	4202.7(12)	9964
Z	4	4
Crystal system	Orthorhombic	Monoclinic
Space group	$P2_12_12_1$	$P2_1/c$
d_{calc}, g/cm^3	1.329	1.420
θ range, °	2.52 to 69.97	2.38 to 74.61
μ, mm^{-1}	3.544	4.988
Abs. Correction	SADABS	TWINABS
GOF	1.111	1.078
R_1,[a] wR_2[b] [I>2 σ(I)]	0.0371, 0.0890	0.0441, 0.1355
Radiation Type	Cu K_α	Cu K_α

[a] $R_1 = \sum||F_o| - |F_c||/\sum|F_o|$. [b] $wR_2 = [\sum[w(F_o^2-F_c^2)^2]/\sum[w(F_o^2)^2]^{1/2}$

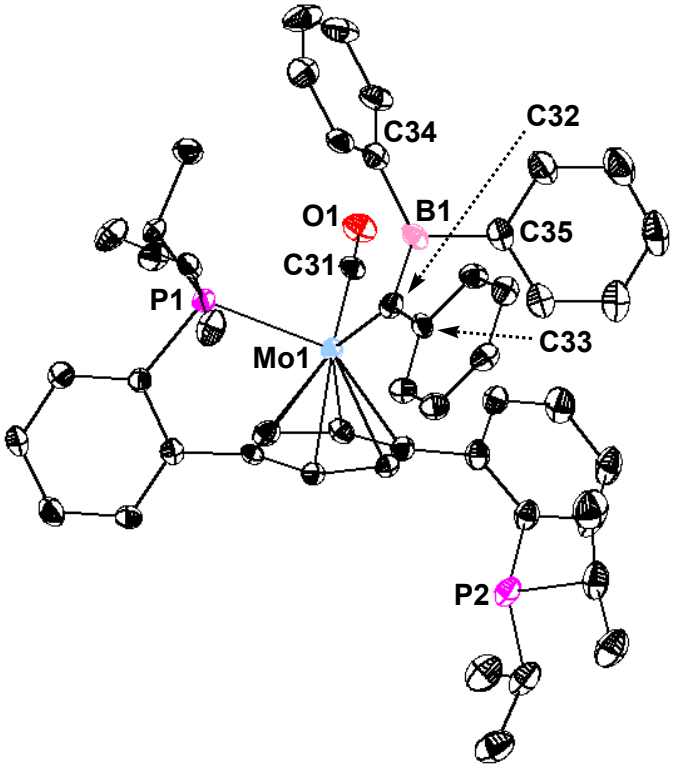

Figure S15—Structural drawing of **6** with 50% probability anisotropic displacement ellipsoids. Hydrogen atoms are omitted for clarity.

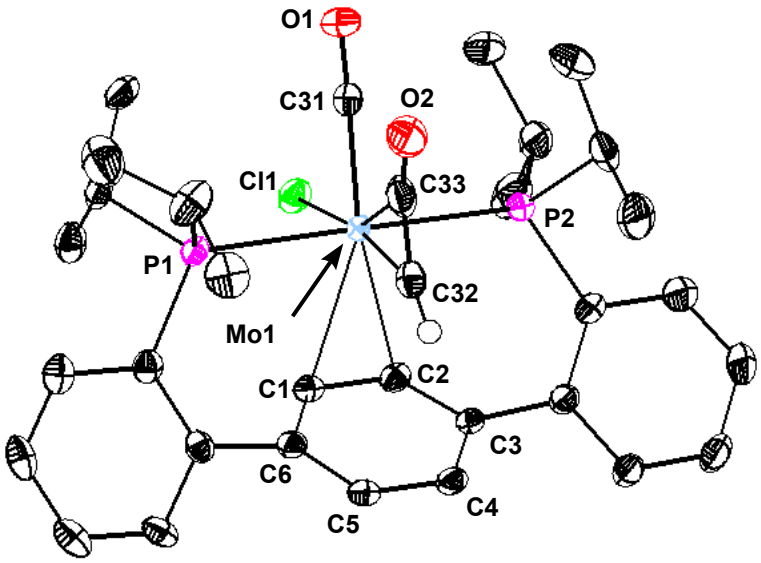

Figure S16—Structural drawing of **7** with 50% probability anisotropic displacement ellipsoids. Hydrogen atoms are omitted for clarity, except for the key ketenyl H, which was located in the electron density map and freely refined. THF solvate omitted for clarity.

REFERENCES

1. Pangborn, A. B.; Giardello, M. A.; Grubbs, R. H.; Rosen, R. K.; Timmers, F. J. Safe and convenient procedure for solvent purification. *Organometallics* **1996,** *15* (5), 1518-1520.
2. Buss, J. A.; Bailey, G. A.; Oppenheim, J.; VanderVelde, D. G.; Goddard, W. A.; Agapie, T. CO Coupling Chemistry of a Terminal Mo Carbide: Sequential Addition of Proton, Hydride, and CO Releases Ethenone. *J. Am. Chem. Soc.* **2019,** *141* (39), 15664-15674.
3. Fulmer, G. R.; Miller, A. J. M.; Sherden, N. H.; Gottlieb, H. E.; Nudelman, A.; Stoltz, B. M.; Bercaw, J. E.; Goldberg, K. I. NMR Chemical Shifts of Trace Impurities: Common Laboratory Solvents, Organics, and Gases in Deuterated Solvents Relevant to the Organometallic Chemist. *Organometallics* **2010,** *29* (9), 2176-2179.
4. Cox, A. P.; Thomas, L. F.; Sheridan, J. Internuclear distances in keten from spectroscopic measurements. *Spectrochimica Acta* **1959,** *15*, 542-543.
5. Churchill, M. R.; Wasserman, H. J.; Holmes, S. J.; Schrock, R. R. Coupling of methylidyne and carbonyl ligands on tungsten. Crystal structure of $W(\eta^2\text{-}HCCOAlCl_3)(CO)(PMe_3)_3Cl$. *Organometallics* **1982,** *1* (5), 766-768.
6. (a) Kreissl, F. R.; Friedrich, P.; Huttner, G. *Angew. Chem. Int. Ed.* 1977**, 16**, 102-103. (b) Fischer, E. O.; Filippou, A. C.; Alt, H. G.; Ackermann, K. *J. Organomet. Chem.* 1983**, 254**, C21-C23. (c) Birdwhistell, K. R.; Tonker, T. L.; Templeton, J. L.; Kenan, W. R. *J. Am. Chem. Soc.* 1985**, 107**, 4474-4483. (d) Chisholm, M. H.; Huffman, J. C.; Marchant, N. S.*J. Chem. Soc., Chem. Commun.* 1986**, 9**, 717-718. (e) Hill, A. F.; Malget, J. M.; White, A. J. P.; Williams, D. J. *Chem Commun.* 1996**, 6**, 721-722. (f) Wadepohl, H.; Arnold, U.; Pritzkow, H.; Calhorda, M. J.; Veiros, L. s. F. *J. Organomet. Chem.* 1999**, 587**, 233-243. (g) Stone, K. C.; Jamison, G. M.; White, P. S.; Templeton, J. L. *Inorg. Chim. Acta* 2002**, 330**, 161-172.
7. Wiedner, E. S.; Chambers, M. B.; Pitman, C. L.; Bullock, R. M.; Miller, A. J. M.; Appel, A. M. Thermodynamic Hydricity of Transition Metal Hydrides. *Chem. Rev.* **2016,** *116* (15), 8655-8692.
8. Gaussian 09, Revision C.01, Frisch, M. J.; Trucks, G. W.; Schlegel, H. B.; Scuseria, G. E.; Robb, M. A.; Cheeseman, J. R.; Scalmani, G.; Barone, V.; Mennucci, B.; Petersson, G. A.; Nakatsuji, H.; Caricato, M.; Li, X.; Hratchian, H. P.; Izmaylov, A. F.; Bloino, J.; Zheng, G.; Sonnenberg, J. L.; Hada, M.; Ehara, M.; Toyota, K.; Fukuda, R.; Hasegawa, J.; Ishida, M.; Nakajima, T.; Honda, Y.; Kitao, O.; Nakai, H.; Vreven, T.; Montgomery, Jr., J. A.; Peralta, J. E.; Ogliaro, F.; Bearpark, M.; Heyd, J. J.; Brothers, E.; Kudin, K. N.; Staroverov, V. N.; Kobayashi, R.; Normand, J.; Raghavachari, K.; Rendell, A.; Burant, J. C.; Iyengar, S. S.; Tomasi, J.; Cossi, M.; Rega, N.; Millam, J. M.; Klene, M.; Knox, J. E.; Cross, J. B.; Bakken, V.; Adamo, C.; Jaramillo, J.; Gomperts, R.; Stratmann, R. E.; Yazyev, O.; Austin, A. J.; Cammi, R.; Pomelli, C.; Ochterski, J. W.; Martin, R. L.; Morokuma, K.; Zakrzewski, V. G.; Voth, G. A.; Salvador, P.; Dannenberg, J. J.; Dapprich, S.; Daniels, A. D.; Farkas, Ö.; Foresman, J. B.; Ortiz, J. V.; Cioslowski, J.; Fox, D. J. Gaussian, Inc., Wallingford CT, 2009.
9. (a) Perdew, J. P.; Ruzsinszky, A.; Csonka, G. I.; Constantin, L. A.; Sun, J. Workhorse Semilocal Density Functional for Condensed Matter Physics and Quantum Chemistry. *Phys. Rev. Lett.* **2009,** *103* (2), 026403. (b) Perdew, J. P.; Ruzsinszky, A.; Csonka, G. I.; Constantin, L. A.; Sun, J. Erratum: Workhorse Semilocal Density Functional for Condensed Matter Physics and Quantum Chemistry [Phys. Rev. Lett. 103, 026403 (2009)]. *Phys. Rev. Lett.* **2011,** *106* (17), 179902.
10.(a) Dunning, T. H.; Hay, P. J., Gaussian Basis Sets for Molecular Calculations. In *Methods of Electronic Structure Theory*, Schaefer, H. F., Ed. Springer US: Boston, MA, 1977; pp 1-27. (b) Hay, P. J.; Wadt, W. R. Ab initio effective core potentials for molecular calculations. Potentials for the transition metal atoms Sc to Hg. *J. Chem. Phys.* **1985,** *82* (1), 270-283. (c) Hay, P. J.; Wadt, W. R. Ab initio effective core potentials for molecular calculations. Potentials for K to Au including the outermost core orbitals. *J. Chem. Phys.* **1985,** *82* (1), 299-310. (d) Wadt, W. R.; Hay, P. J. Ab initio effective core potentials for molecular calculations. Potentials for main group elements Na to Bi. *J. Chem. Phys.* **1985,** *82* (1), 284-298.
11.Miertuš, S.; Scrocco, E.; Tomasi, J. Electrostatic interaction of a solute with a continuum. A direct utilizaion of AB initio molecular potentials for the prevision of solvent effects. *Chem. Phys.* **1981,** *55* (1), 117-129.

12. Pascual-ahuir, J. L.; Silla, E.; Tuñon, I. GEPOL: An improved description of molecular surfaces. III. A new algorithm for the computation of a solvent-excluding surface. *J. Comput. Chem.* **1994,** *15* (10), 1127-1138.
13. Miertuš, S.; Tomasi, J. Approximate evaluations of the electrostatic free energy and internal energy changes in solution processes. *Chem. Phys.* **1982,** *65* (2), 239-245.
14. Pettersen, E. F.; Goddard, T. D.; Huang, C. C.; Couch, G. S.; Greenblatt, D. M.; Meng, E. C.; Ferrin, T. E. UCSF Chimera—A visualization system for exploratory research and analysis. *J. Comput. Chem.* **2004,** *25* (13), 1605-1612.
15. APEX3, Version 1 User Manual, M86-EXX229, Bruker Analytical X-ray Systems, Madison, WI, May 2016.
16. Sheldrick, G.M. "SADABS (version 2008/1): Program for Absorption Correction for Data from Area Detector Frames", University of Göttingen, 2008.
17. Dolomanov, O. V.; Bourhis, L. J.; Gildea, R. J.; Howard, J. A. K.; Puschmann, H. OLEX^2: a complete structure solution, refinement and analysis program. *J. Appl. Cryst.* **2009,** *42* (2), 339-341.
18. Sheldrick, G. Crystal structure refinement with SHELXL. *Acta Crystallographica Section C* **2015,** *71* (1), 3-8.
19. Brandenburg, K. (1999). DIAMOND. Crystal Impact GbR, Bonn, Germany.
20. Sheldrick, G. Cell_Now and TWINABS. *University of Göttingen, Germany* **2008**.